A Mononuclear Nonheme Iron(III)-Peroxo Complex with an Unprecedented High O-O Stretch and Electrophilic Reactivity

Wenjuan Zhu,[†] Semin Jang,[†] Jin Xiong,[‡] Roman Ezhov,[§] Xiao-Xi Li,[†] Taeyeon Kim,[†] Mi Sook Seo,[†] Yong-Min Lee,[†] Yulia Pushkar,[§] Ritimukta Sarangi,[¶,*] Yisong Guo,[‡,*] and Wonwoo Nam[†,#,*]

[†] Department of Chemistry and Nano Science, Ewha Womans University, Seoul 03760, Korea
[‡] Department of Chemistry, Carnegie Mellon University, Pittsburgh, Pennsylvania 15213, United States
[§] Department of Physics and Astronomy, Purdue University, West Lafayette, IN 47907, United States
[¶] Stanford Synchrotron Radiation Lightsource, SLAC National Accelerator Laboratory, Stanford, California 94025, United States
[#] School of Chemistry and Chemical Engineering, University of Jinan, Jinan 250022, China

ABSTRACT: A mononuclear nonheme iron(III)-peroxo complex, $[Fe(III)(O_2)(13\text{-TMC})]^+$ (**1**), was synthesized and characterized spectroscopically; the characterization with EPR, Mössbauer, XAS, mass, and resonance Raman spectroscopies supported a high-spin $S = 5/2$ Fe(III) species binding an O_2-unit. A notable observation was an unusually high $\nu_{O\text{-}O}$ at ~1000 cm^{-1} for the peroxo ligand. In reactivities, **1** showed an electrophilic reactivity in hydrogen atom (H-atom) abstraction and oxygen atom transfer (OAT) reactions. In the H-atom reaction, a kinetic isotope effect (KIE) value of 5.8 was obtained in the oxidation of 9,10-dihydroanthracene. In the OAT reaction, a negative ρ value of –0.61 in Hammett plot was determined in the oxidation of *para*-X-substituted thioanisoles. Another interesting observation was the electrophilic reactivity of **1** in the oxidation of benzaldehyde derivatives, such as a negative ρ value of –0.77 in Hammett plot and a KIE value of 2.2. To the best of our knowledge, the present study reports the first example of a mononuclear nonheme iron(III)-peroxo complex with an unusually high $\nu_{O\text{-}O}$ value and an unprecedented electrophilic reactivity in oxidation reactions.

Metalloenzymes and synthetic metal catalysts utilize metal-oxygen intermediates, such as metal-oxo, -hydroperoxo, -peroxo, and -superoxo species, as active oxidants in biological and chemical transformations of organic substrates.[1] While high-valent metal-oxo intermediates have been well investigated in heme and nonheme systems,[2,3] other metal-oxygen intermediates containing an O_2-unit are less clearly understood in chemical reactions.[4] In reactivities, mononuclear metal-peroxo species are nucleophiles that conduct nucleophilic oxidative reactions,[5] whereas metal-superoxo species are electrophiles that can abstract an H-atom from substrate C-H bonds.[6,7]

In nonheme iron enzymes, such as Rieske *cis*-diol dioxygenases, extradiol dioxygenases, 2-oxo acid dioxygenases, and isopenicillin *N*-synthase, iron-O_2 intermediates have been invoked as active oxidants in various biological reactions.[8] In many of those enzymatic reactions, iron-superoxo species have been proposed as active oxidants that effect the H-atom abstraction in the catalytic cycles;[9] iron-peroxo species were excluded as a potent intermediate in those biological reactions since iron-peroxo species are nucleophiles and cannot conduct electrophilic reactions, such as an H-atom abstraction from substrate C-H bonds and an OAT to organic substrates.[5]

Scheme 1. DFT-Optimized Structure, Spectroscopic Characterization, and Reactivity of $[Fe(III)(O_2)(13\text{-TMC})]^+$ (1)

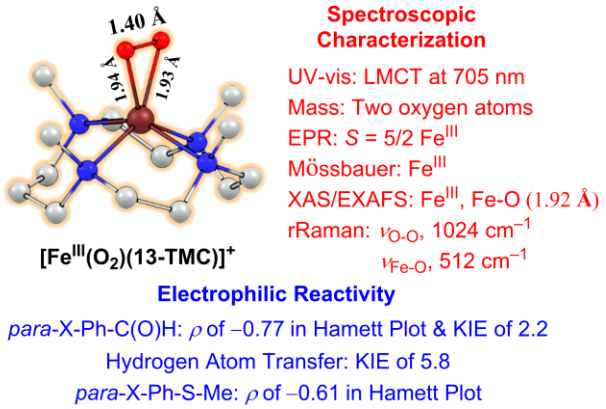

Recently, Sastri, de Visser, and co-workers reported an elegant result showing that nonheme manganese(III)-peroxo complexes, characterized with UV-vis spectrophotometer and electrospray ionization mass spectrometry, were capable of deformylating aldehydes, such as 2-phenylpropionaldehyde (2-PPA) and α-[D_1]-2-phenylpropionaldehyde (α-[D_1]-PPA), via an initial H-atom abstraction, affording a large kinetic isotope effect (KIE) of 5.4.[10] This result indicates that the deformylation reaction occurs via an electrophilic H-atom abstraction of aldehyde C(O)-H bond by the Mn(III)-peroxo complexes. However, interestingly, these Mn(III)-peroxo complexes cannot abstract an H-atom from hydrocarbons, such as 1,4-cyclohexadiene.[10b] In addition, no OAT reactions were demonstrated by these Mn(III)-peroxo complexes.

In biomimetic systems, a number of mononuclear nonheme iron(III)-peroxo complexes have been synthesized and characterized spectroscopically and structurally;[11-14] a notable example is an X-ray crystal structure of an iron(III)-peroxo complex bearing a macrocyclic 14-TMC[15] ligand, $[Fe(III)(O_2)(14\text{-TMC})]^+$.[11] In many of the iron(III)-peroxo complexes, the $\nu_{Fe\text{-}O}$ and $\nu_{O\text{-}O}$ stretches have been observed at ~490 and ~820 cm^{-1}, respectively, in resonance Raman (rRaman) experiments.[11,12,13c,13f,14]

In reactivity studies, nonheme iron(III)-peroxo complexes have shown nucleophilic reactivities, such as in aldehyde deformylation reactions,[11,14] as reported in heme models.[5] Herein, we report for the first time the synthesis, characterization, and reactivity studies of a mononuclear nonheme iron(III)-peroxo complex bearing a macrocyclic 13-TMC[15] ligand, $[Fe(III)(O_2)(13\text{-TMC})]^+$ (**1**), with an unusual high O-O stretching mode and an unprecedented electrophilic reactivity in oxidation reactions (see Scheme 1).

The iron(III)-peroxo complex, **1**, was synthesized by reacting $Fe(II)(13\text{-TMC})(CF_3SO_3)_2$ (1.0 mM) with 10 equiv of H_2O_2 in the presence of 5.0 equiv of triethylamine in 2,2,2-trifluoroethanol (TFE) at −10 °C. The intermediate **1**, which was metastable ($t_{1/2}$ ~ 30 min) at −10 °C, was characterized with various spectroscopic techniques, such as UV-vis spectrophotometry, cold-spray ionization mass spectrometry (CSI-MS), electron paramagnetic resonance (EPR), rRaman, Mössbauer and X-ray absorption spectroscopy (XAS). The UV-vis spectrum of **1** shows a broad absorption band at 705 nm (Figure 1a; Figure S1), which is typically assigned to a ligand-to-metal charge transfer (LMCT) transition from the O_2^{2-} unit to Fe^{III} in mononuclear nonheme iron(III)-peroxo complexes.[11-14] CSI-MS data shows a mass peak at *m/z* 330.1 corresponding to $[Fe(^{16}O_2)(13\text{-TMC})]^+$. This shifts to *m/z* 334.1 (corresponding to $[Fe(^{18}O_2)(13\text{-TMC})]^+$) when **1** was prepared with $H_2{}^{18}O_2$ (Figure 1b), suggesting that **1** contains two oxygen atoms (i.e., an O_2 unit). X-band EPR spectrum of **1** exhibits an intense signal centered at g = 4.3, typical of a high-spin (S = 5/2) Fe(III) species (Figures S2 and S3).[11-14]

The rRaman spectrum of **1**, excited at 785 nm in frozen TFE solution, exhibits two isotope sensitive bands at 512 and 1024 cm^{-1}, which shift to 489 and 975 cm^{-1}, respectively, with ^{18}O-labeled **1** (Figure 1c; Figure S4 for other solvents). The bands at 512 and 1024 cm^{-1} are assigned as Fe-O and O-O stretching vibrations, respectively. It is notable that the $^{16}\Delta - {}^{18}\Delta$ value of 49 cm^{-1} is smaller than that predicted by Hooke's law calculations for the O-O vibration at 1024 cm^{-1} ($^{16}\Delta - {}^{18}\Delta$ (calculated) = 59 cm^{-1})[15] and that the O-O stretching vibration of **1** at ~1000 cm^{-1} is much higher than those of other mononuclear nonheme iron(III)-peroxo complexes.[11,12,13b,13c,13f,14] For example, $[Fe(III)(O_2)(14\text{-TMC})]^+$, bearing a TMC ligand with a different macrocyclic ring size, exhibits an O-O stretching vibration at 825 cm^{-1}. Thus, the difference in ring size of the macrocyclic TMC ligand in $[Fe(III)(O_2)(n\text{-TMC})]^+$ affords a dramatic change in the O-O stretching vibration (825 cm^{-1} for $[Fe(III)(O_2)(14\text{-TMC})]^+$ and 1024 cm^{-1} for **1**) and a change in the Fe-O stretching vibration (487 cm^{-1} for $[Fe(III)(O_2)(14\text{-TMC})]^+$ and 512 cm^{-1} for **1**). It is also noted that late transition metal-peroxo complexes bearing *n*-TMC ligands exhibit their O-O stretching vibrations at ~1000 cm^{-1}, such as $[Ni(III)(O_2)(12\text{-TMC})]^+$ and $[Ni(III)(O_2)(13\text{-TMC})]^+$ at 1002 and 1008 cm^{-1}, respectively.[15,17]

Mössbauer data were measured on complex **1** and reveal that a majority of the iron (~80%) in the Mössbauer sample containing **1** exhibited paramagnetic features originating from a single S = 5/2 species (Figure 2a). The remaining ~20% iron in the sample exhibited quadrupole doublet features (see the SI for additional discussion). The overall spectral simulations by using an S = 5/2 spin Hamiltonian on the spectra measured at 4.2 K with applied fields of 45 mT and 7 T are shown in Figure 2a and Figure S5. The simulation[18] revealed that the isomer shift of the S = 5/2 species is 0.52 mm/s, thus confirming that complex **1** is a high-spin ferric

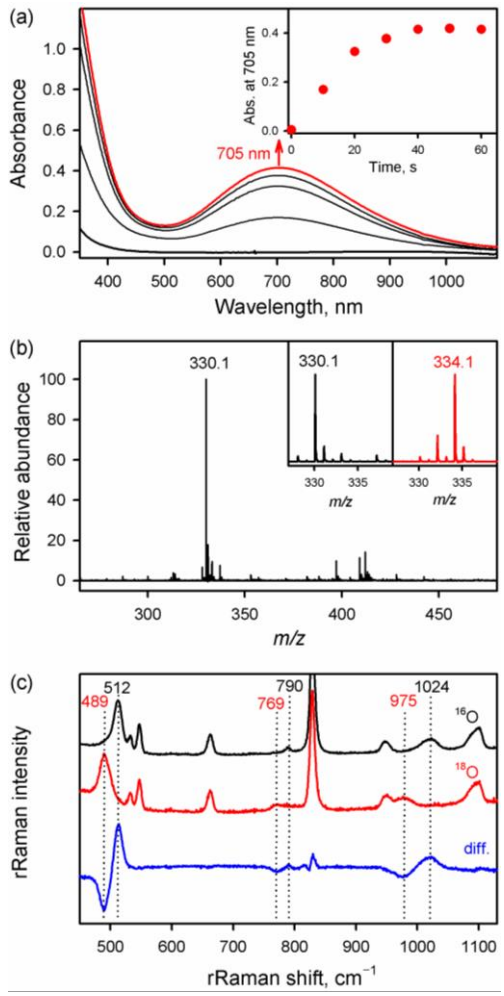

Figure 1. (a) UV-vis spectral changes showing the formation of **1** upon addition of H_2O_2 (10 mM) to a solution containing $[Fe^{II}(13\text{-TMC})]^{2+}$ (1.0 mM) and triethylamine (5.0 mM) in TFE at −10 °C. (b) Cold-spray ionization mass spectrum of **1**. Insets show observed isotope distribution patterns for $[Fe(III)(^{16}O_2)(13\text{-TMC})]^+$ (left panel) and $[Fe(III)(^{18}O_2)(13\text{-TMC})]^+$ (right panel). (c) rRaman spectra of **1** in TFE with ^{16}O (black) and ^{18}O (red) isotopic substitution in the region of Fe-O and O-O stretches (λ_{ex} = 785 nm, 77 K). Blue is the ^{16}O and ^{18}O difference. The peak at 790 cm^{-1} may be from an impurity, such as an iron(III)-OOH species.[12-14]

species. The results on **1** are comparable to those reported for $[Fe(III)(O_2)(14\text{-TMC})]^+$.[19]

Fe K-edge X-ray absorption spectroscopic (XAS) studies of **1** are presented in Figure 2b. Formation of **1** causes an ~3.5 eV shift of the absorption edge to higher energy. Pre-edge feature at ~7111.5 eV in $Fe(II)(13\text{-TMC})(CF_3SO_3)_2$ shifts to ~7113.5 eV in **1**. These shifts are consistent with a one-electron oxidation of the iron center in **1** to Fe(III). The extended X-ray absorption fine structure (EXAFS) region of **1** was modeled as six-coordinate iron with two Fe-O bonds (1.92 Å) and four Fe-N bonds (2.20 Å) (Figure 2c, Table S1). Collectively, the spectroscopic data discussed above unambiguously assign **1** as an iron(III)-peroxo complex, $[Fe(III)(O_2)(13\text{-TMC})]^+$, with an S = 5/2 spin state. Its geometric structure derived from Fe K-edge EXAFS is reproduced well by DFT calculations and is presented in Scheme 1 (see SI for the detailed calculations; Tables S2 and S3 and Figure S6).

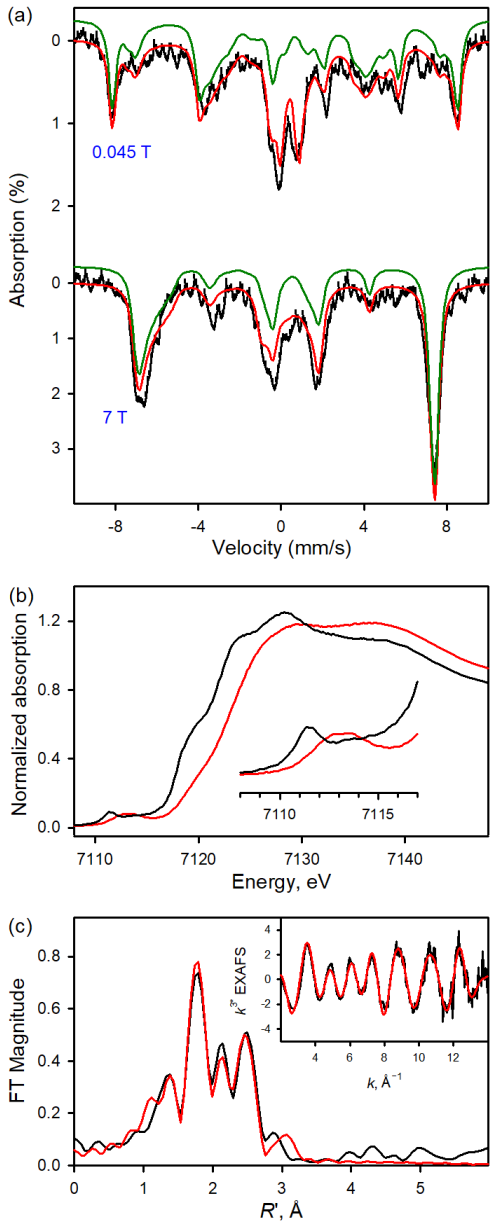

Figure 2. (a) 4.2 K Mössbauer spectra (black vertical bars) with the applied magnetic fields of 0.045 T (top) and 7 T (bottom) and their overall spectral simulations (red lines) for **1**. The simulations of the iron species representing ~80% of the total iron in the sample are indicated in the green lines.[17] (b) Normalized Fe K-edge XAS data for $Fe^{II}(13\text{-TMC})(CF_3SO_3)_2$ (black) and **1** (red). The inset shows the expanded pre-edge region. (c) Nonphase-shift corrected Fourier transform (FT) data (black line) and the corresponding FEFF fit (red line) to the Fe K-edge FT data for **1**. The inset shows the EXAFS data (black line) and fit (red line).

We then performed the reactivity studies of **1** in oxidation reactions. First, the reactivity of **1** was examined in nucleophilic oxidative reactions, such as the oxidation of benzaldehyde derivatives, with a prediction that **1** should react with benzaldehyde derivatives via a nucleophilic addition (NA) (Scheme 2, pathway *a*) and a positive ρ value would be observed in Hammett plot.[4b,5,11,20] With that in mind, we carried out the reaction of **1** with benzaldehyde derivatives in TFE at −10 °C; **1** disappeared upon the addition of benzaldehyde and the rate of the disappearance of **1** increased linearly with the increase of the benzaldehyde concentration (Figure S7). Similarly, the second-order rate

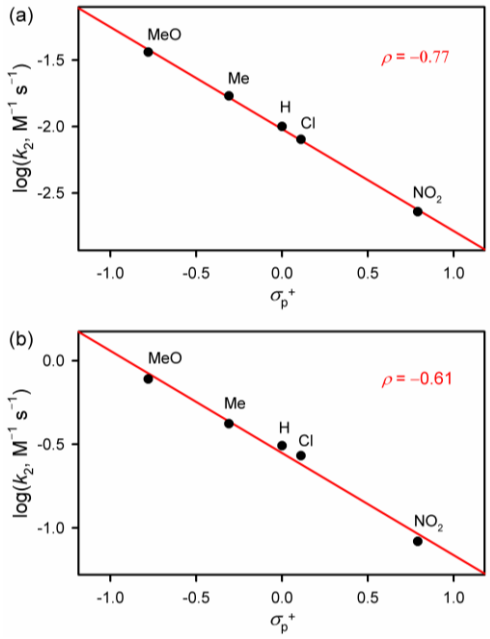

Figure 3. Hammett plots of log k_2 against the σ_p^+ values of *para*-X-substituents of substrates in the oxidation of (a) *para*-X-substituted benzaldehydes and (b) *para*-X-substituted thioanisoles by **1** in TFE at −10 °C.

Scheme 2. Reaction Pathways, HAT versus NA, of an Iron(III)-Peroxo Intermediate

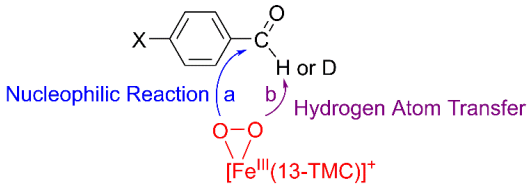

constants with *para*-X-substituted benzaldehydes were determined (Figure S8). Interestingly, when the rate constants (log k_2) were plotted against Hammett parameters (σ_p^+) of substituents, a negative ρ value of −0.77 was obtained in the Hammett plot (Figure 3a; also see Figure S9 for the plot of log k_2 against the C(O)-H BDEs of substituted benzaldehydes). This result is surprising and suggesting that **1** possesses an electrophilic reactivity, which is different from the nucleophilic reactivity of other metal-peroxo species.[5,11,20] More interestingly, a KIE value of 2.2 was obtained in the oxidation of benzaldehyde and deuterated benzaldehyde [e.g., PhC(=O)H and PhC(=O)D] (Figure S7b), indicating that the oxidation of benzaldehydes by **1** occurs via a H(D)-atom abstraction of PhC(=O)H and PhC(=O)D (Scheme 2, pathway *b*). In the oxidation of benzaldehyde by **1**, benzoic acid (65(3)%) as a sole organic product and iron(II) species as a decay product of **1** were produced (Figure S10). If the reaction of **1** and benzaldehyde occurs via a NA of the O_2 group to the carbonyl group of benzaldehyde (Scheme 2, pathway *a*), the KIE value should be ≤1.[5,11,20] We therefore conclude that **1** reacts with benzaldehyde by abstracting an H-atom via an electrophilic oxidative pathway (Scheme 2, pathway *b*).

With the observations that **1** is an electrophilic oxidant and can abstract an H-atom from benzaldehyde, we conducted the C-H bond activation reactions with 1,4-cyclohexadiene (CHD, 78 kcal

mol^{-1}), 9,10-dihydroanthracene (DHA, 77 kcal mol^{-1}), xanthene (75.5 kcal mol^{-1}), and 10-methyl-9,10-dihydroacridine ($AcrH_2$, 73.7 kcal mol^{-1}).[21] Addition of DHA to a solution of **1** resulted in the disappearance of the intermediate and the reaction rate increased with the increase of the substrate concentration, affording a second-order rate constant of 7.5×10^{-2} M^{-1} s^{-1} in TFE/MC (v/v 3:1) at –10 °C (Figure S11). We also obtained a KIE value of 5.8(3) in the C-H bond activation of DHA-h_4 and DHA-d_4 (Figure S11b). In the reaction of **1** with DHA, anthracene (48(2)%) with iron(II) species was produced (Figures S12 and S13). The second-order rate constants with other substrates, such as $AcrH_2$, xanthene, and CHD, were also determined (Figure S14), showing the decrease of the k_2 values with the increase of the BDEs of substrates C-H bonds (Figure S15). In the oxidation of $AcrH_2$, xanthene, and CHD by **1**, $AcrH^+$ (92(4)%), xanthone (38(4)%), and benzene (42(5)%) were yielded as products, respectively.[22] These results clearly suggest that an H-atom abstraction from the substrates C-H bond by **1** is the rate-determining step, as observed in the benzaldehyde oxidation reaction by **1** (vide supra).

The OAT reaction of **1** was also performed with *para*-X-substituted thioanisoles. As observed in the benzaldehyde and C-H bond activation reactions, **1** disappeared upon the addition of thioanisole (Figure S16a), and the rate of the disappearance of **1** increased with the increase of thioanisole concentration (Figure S16b). In this reaction, methyl phenyl sulfoxide (63(4)%) was yielded with iron(III) species as a decay product of **1** (Figures S17 and S18).[23] Similarly, the second-order rate constants with *para*-X-substituted thioanisoles were also determined (Figure S19), and we obtained a negative ρ value of –0.61 in Hammett plot when the rate constants (log k_2) were plotted against Hammett constants (σ_p^+) of substituents (Figure 3b). The one-electron reduction potential (E_{red}) of **1** was also determined to be 0.44 V vs SCE (Figure S20).[24,25] These results led us to conclude that **1** is capable of conducting OAT reactions with an electrophilic reactivity.

In conclusion, we have reported for the first time a mononuclear nonheme iron(III)-peroxo complex, $[Fe(III)(O_2)(13\text{-TMC})]^+$ (**1**), with an unusually high $\nu_{O\text{-}O}$ at ~1000 cm^{-1} and an unprecedented electrophilic reactivity in the C-H bond activation and OAT reactions as well as in the oxidation of benzaldehyde in nonheme iron systems. The observation of the unexpected electrophilic reactivity of **1** leads us to suggest that nonheme iron-peroxo intermediates can conduct electrophilic oxidation reactions in nonheme iron enzymes and biomimetic models, which has never been considered and/or discussed previously. In future studies, detailed mechanisms of the HAT and OAT reactions by the mononuclear nonheme iron(III)-peroxo complex will be investigated experimentally and theoretically. We will also attempt to find more examples of synthetic iron-peroxo complexes in electrophilic oxidation reactions. The effect of the macrocyclic ring size on the physical and chemical properties of the O_2-unit in $[Fe(III)(O_2)(n\text{-TMC})]^+$ complexes is under investigation in this laboratory.

ASSOCIATED CONTENT

Supporting Information

The Supporting Information is available free of charge via the Internet at http://pubs.acs.org.

Experimental Section, Table S1 – S3, Figures S1 – S20, and Calculated Cartesian Coordinates (PDF).

AUTHOR INFORMATION

Corresponding Author

wwnam@ewha.ac.kr
ysguo@andrew.cmu.edu
ritis@slac.stanford.edu

Notes

The authors declare no competing financial interests.

ACKNOWLEDGMENT

This work was supported by the NRF of Korea (NRF-2021R1A3B1076539 to W.N. and NRF-2020R1I1A1A01074630 to Y.-M.L.). This research was also supported by NSF (CHE-2004147 to Y.P. and CHE-1654060 to Y.G.). The SSRL Structural Molecular Biology Program is supported by the DOE Office of Biological and Environmental Research, and by the National Institutes of Health, National Institute of General Medical Sciences (P30GM133894). W.Z. thanks to China Scholarship Council (CSC201908360192)

REFERENCES

(1) (a) Nam, W. Dioxygen Activation by Metalloenzymes and Models. *Acc. Chem. Res.* **2007**, *40*, 465 and references therein. (b) Que, L. 60 Years of Dioxygen Activation. *J. Biol. Inorg. Chem.* **2017**, *22*, 171–173 and references therein.

(2) (a) Dubey, K. D.; Shaik, S. Cytochrome P450 – The Wonderful Nanomachine Revealed through Dynamic Simulations of the Catalytic Cycle. *Acc. Chem. Res.* **2019**, *52*, 389–399. (b) Moody, P. C. E.; Raven, E. L. The Nature and Reactivity of Ferryl Heme in Compounds I and II. *Acc. Chem. Res.* **2018**, *51*, 427–435. (c) Huang, X.; Groves, J. T. Oxygen Activation and Radical Transformations in Heme Proteins and Metalloporphyrins. *Chem. Rev.* **2018**, *118*, 2491–2553.

(3) (a) Larson, V. A.; Battistella, B.; Ray, K.; Lehnert, N.; Nam, W. Iron and Manganese Oxo Complexes, Oxo Wall and Beyond. *Nat. Rev. Chem.* **2020**, *4*, 404–419. (b) Banerjee, R.; Jones, J. C.; Lipscomb, J. D. Soluble Methane Monooxygenase. *Annu. Rev. Biochem.* **2019**, *88*, 409–431. (c) Guo, M.; Corona, T.; Ray, K.; Nam, W. Heme and Nonheme High-Valent Iron and Manganese Oxo Cores in Biological and Abiological Oxidation Reactions. *ACS Cent. Sci.* **2019**, *5*, 13–28.

(4) (a) Fukuzumi, S.; Cho, K.-B.; Lee, Y.-M.; Hong, S.; Nam, W. Mechanistic Dichotomies in Redox Reactions of Mononuclear Metal-Oxygen Intermediates. *Chem. Soc. Rev.* **2020**, *49*, 8988–9027. (b) Cho, J.; Sarangi, R.; Nam, W. Mononuclear Metal-O_2 Complexes Bearing Macrocyclic *N*-Tetramethylated Cyclam Ligands. *Acc. Chem. Res.* **2012**, *45*, 1321–1330.

(5) Wertz, D. L.; Valentine, J. S. Nucleophilicity of Iron-Peroxo Porphyrin Complexes. *Struct. Bonding* 2000, *97*, 37–60.

(6) (a) Noh, H.; Cho, J. Synthesis, Characterization and Reactivity of Non-Heme 1st Row Tansitition Metal-Superoxo Intermediates. *Coord. Chem. Rev.* **2019**, *382*, 126–144. (b) Fukuzumi, S.; Lee, Y.-M.; Nam, W. Structure and Reactivity of the First-Row d-Block Metal-Superoxo Complexes. *Dalton Trans.* **2019**, *48*, 9469–9489. (c) Sankaralingam, M.; Lee, Y.-M.; Nam, W.; Fukuzumi, S. Amphoteric Reactivity of Metal-Oxygen Complexes in Oxidation Reactions. *Coord. Chem. Rev.* **2018**, *365*, 41–59. (d) Ure, A. D.; McDonald, A. R. Nucleophilic Reactivity of a Metal-Bound Superoxide Ligand. *Synlett* **2015**, *26*, 2060–2066.

(7) (a) Lin, Y.-H.; Kutin, Y.; van Gastel, M.; Bill, E.; Schnegg, A.; Ye, S.; Lee, W.-Z. A Manganese(IV)-Hydroperoxo Intermediate Generated by Protonation of the Corresponding Manganese(III)-Superoxo Complex. *J. Am. Chem. Soc.* **2020**, *142*, 10255–10260. (b) Panda, C.; Chandra, A.; Corona, T.; Andris, E.; Pandey, B.; Garai, S.; Lindenmaier, N.; Künstner, S.; Farquhar, E. R.; Roithová, J.; Rajaraman, G.; Driess, M.; Ray, K. Nucleophilic versus Electrophilic Reactivity of Bioinspired Superoxido Nickel(II) Complexes. *Angew. Chem., Int. Ed.* **2018**, *57*, 14883–14887. (c) Wang, C.-C.; Chang, H.-C.; Lai, Y.-C.; Fang, H.; Li, C.-C.; Hsu, H.-K.; Li, Z.-Y.; Lin, T.-S.; Kuo, T.-S.; Neese, F.; Ye, S.; Chiang, Y.-W.; Tsai, M.-L.; Liaw, W.-F.; Lee, W.-Z. A Structurally Characterized Nonheme Cobalt-Hydroperoxo Complex Derived from Its Superoxo Intermediate via Hydrogen Atom Abstraction. *J. Am. Chem. Soc.* **2016**, *138*,

14186–14189. (d) Hong, S.; Sutherlin, K. D.; Park, J.; Kwon, E.; Siegler, M. A.; Solomon, E. I.; Nam, W. Crystallographic and Spectroscopic Characterization and Reactivities of a Mononuclear Non-Haem Iron(III)-Superoxo Complex. *Nat. Commun.* **2014**, *5*, 5440. (e) Pirovano, P.; Magherusan, A. M.; McGlynn, C.; Ure, A.; Lynes, A.; McDonald, A. R. Nucleophilic Reactivity of a Copper(II)-Superoxide Complex. *Angew. Chem., Int. Ed.* **2014**, *53*, 5946–5950.

(8) Kovaleva, E. G.; Lipscomb, J. D. Versatility of Biological Non-Heme Fe(II) Centers in Oxygen Activation Reactions. *Nat. Chem. Biol.* **2008**, *4*, 186–193.

(9) (a) van der Donk, W. A.; Krebs, C.; Bollinger, J. M., Jr. Substrate Activation by Iron Superoxo Intermediates. *Curr. Opin. Struct. Biol.* **2010**, *20*, 673–683. (b) Solomon, E. I.; Goudarzi, S.; Sutherlin, K. D. O_2 Activation by Non-Heme Iron Enzymes. *Biochemistry* **2016**, *55*, 6363–6374.

(10) (a) Barman, P.; Upadhyay, P.; Faponle, A. S.; Kumar, J.; Nag, S. S.; Kumar, D.; Sastri, C. V.; de Visser, S. P. Deformylation Reaction by a Nonheme Manganese(III)-Peroxo Complex via Initial Hydrogen-Atom Abstraction. *Angew. Chem., Int. Ed.* **2016**, *55*, 11091–11095. (b) Cantú Reinhard, F. G.; Barman, P.; Mukherjee, G.; Kumar, J.; Kumar, D.; Kumar, D.; Sastri, C. V.; de Visser, S. P. Keto-Enol Tautomerization Triggers an Electrophilic Aldehyde Deformylation Reaction by a Nonheme Manganese(III)-Peroxo Complex. *J. Am. Chem. Soc.* **2017**, *139*, 18328–18338. (c) Barman, P.; Cantú Reinhard, F. G.; Bagha, U. K.; Kumar, D.; Sastri, C. V.; de Visser, S. P. Hydrogen by Deuterium Substitution in an Aldehyde Tunes the Regioselectivity by a Nonheme Manganese(III)-Peroxo Complex. *Angew. Chem., Int. Ed.* **2019**, *58*, 10639–10643.

(11) Cho, J.; Jeon, S.; Wilson, S. A.; Liu, L. V.; Kang, E. A.; Braymer, J. J.; Lim, M. H.; Hedman, B.; Hodgson, K. O.; Valentine, J. S.; Solomon, E. I.; Nam, W. Structure and Reactivity of a Mononuclear Non-Haem Iron(III)-Peroxo Complex. *Nature* **2011**, *478*, 502–505.

(12) (a) Girerd, J.-J.; Banse, F.; Simaan, A. J. Characterization and Properties of Non-Heme Iron Peroxo Complexes. *Struct. Bonding* 2000, *97*, 143–177. (b) Costas, M.; Mehn, M. P.; Jensen, M. P.; Que, L., Jr. Dioxygen Activation at Mononuclear Nonheme Iron Active Sites: Enzymes, Models, and Intermediates. *Chem. Rev.* **2004**, *104*, 939–986.

(13) (a) Jensen, K. B.; McKenzie, C. J.; Nielsen, L. P.; Pedersen, J. Z.; Svendsen, H. M. Deprotonation of Low-Spin Mononuclear Iron(III)-Hydroperoxide Complexes Give Transient Blue Species Assigned to High-Spin Iron(III)-Peroxide Complexes. *Chem. Commun.* **1999**, 1313–1314. (b) Ho, R. Y. N.; Roelfes, G.; Hermant, R.; Hage, R.; Feringa, B. L.; Que, L., Jr. Resonance Raman Evidence for the Interconversion between an $[Fe^{III}\text{-}\eta^1\text{-}OOH]^{2+}$ and $[Fe^{III}\text{-}\eta^2\text{-}O_2]^+$ Species and Mechanistic Implications Thereof. *Chem. Commun.* **1999**, 2161–2162. (c) Simaan, A. J.; Döpner, S.; Banse, F.; Bourcier, S.; Bouchoux, G.; Boussac, A.; Hildebrandt, P.; Girerd, J.-J. Fe^{III}-Hydroperoxo and Peroxo Complexes with Aminopyridyl Ligands and the Resonance Raman Spectroscopic Identification of the Fe-O and O-O Stretching Modes. *Eur. J. Inorg. Chem.* **2000**, 1627–1633. (d) Simaan, A. J.; Banse, F.; Girerd, J.-J.; Wieghardt, K.; Bill, E. The Electronic Structure of Non-Heme Iron(III)-Hydroperoxo and Iron(III)-Peroxo Model Complexes Studied by Mössbauer and Electron Paramagnetic Resonance Spectroscopies. *Inorg. Chem.* **2001**, *40*, 6538–6540. (e) Horner, O.; Jeandey, C.; Oddou, J.-L; Bonville, P.; McKenzie, C. J.; Lotour, J.-M. Hydrogenperoxo-$[(bztpen)Fe(OOH)]^{2+}$ and Its Deprotonation Product Peroxo-$[(bztpen)Fe(O_2)]^+$, Studied by EPR and Mössbauer Spectroscopy – Implications for the Electronic Structures of Peroxo Model Complexes. *Eur. J. Inorg. Chem.* **2002**, *12*, 3278–3283. (f) Bukowski, M. R.; Comba, P.; Limberg, C.; Merz, M.; Que, L., Jr.; Wistuba, T. Bispidine Ligand Effects on Iron/Hydrogen Peroxide Chemistry. *Angew. Chem., Int. Ed.* **2004**, *43*, 1283–1287.

(14) Mukherjee, G.; Sastri, C. V. Eccentricities in Spectroscopy and Reactivity of Non-Heme Metal Intermediates Contained in Bispidine Scaffolds. *Isr. J. Chem.* **2020**, *60*, 1032–1048.

(15) Abbreviations used: 14-TMC, 1,4,8,11-tetramethyl-1,4,8,11-tetraazacyclotetradecane; 13-TMC, 1,4,7,10-tetramethyl-1,4,7,10-tetraazacyclotridecane; 12-TMC, 1,4,7,10-tetramethyl-1,4,7,10-tetraazacyclododecane.

(16) There are several examples showing smaller experimental $^{16}\Delta - {}^{18}\Delta$ values than those calculated for Fe-O and O-O vibrations in nonheme Fe-OOR species: (a) Ho, R. Y. N.; Roelfes, G.; Feringa, B. L.; Que, L., Jr. Raman Evidence for a Weakened O-O Bond in Mononuclear Low-Spin Iron(III)-Hydroperoxides. *J. Am. Chem. Soc.* **1999**, *121*, 264–265. (b) Zang, Y.; Kim, J.; Dong, Y.; Wilkinson, E. C.; Appelman, E. H.; Que, L., Jr. Models for Nonheme Iron Intermediates: Structural Basis for Tuning the Spin States of Fe(TPA) Complexes. *J. Am. Chem. Soc.* **1997**, *119*, 4197–4205.

(17) (a) Cho, J.; Sarangi, R.; Annaraj, J.; Kim, S. Y.; Kubo, M.; Ogura, T.; Solomon, E. I.; Nam, W. Geometric and Electronic Structure and Reactivity of a Mononuclear 'Side-On' Nickel(III)-Peroxo Complex. *Nat. Chem.* **2009**, *1*, 568–572. (b) Cho, J.; Kang, H. Y.; Liu, L. V.; Sarangi, R.; Solomon, E. I.; Nam, W. Mononuclear Nickel(II)-Superoxo and Nickel(III)-Peroxo Complexes Bearing a Common Macrocyclic TMC Ligand. *Chem. Sci.* **2013**, *4*, 1502–1508.

(18) Full simulation parameters: $S = 5/2$, $D = -0.2\ cm^{-1}$, $E/D = 0.22$, $A_x/g_n\beta_n = -19.0$ T, $A_y/g_n\beta_n = -20.5$ T, $A_z/g_n\beta_n = -21.0$ T, $\delta = 0.52$ mm/s, $\Delta E_Q = -1.1$ mm/s, and $\eta = -2.2$.

(19) Li, F. F.; Meier, K. K.; Cranswick, M. A.; Chakrabarti, M.; Van Heuvelen, K. M.; Münck, E.; Que, L., Jr. Characterization of a High-Spin Non-Heme Fe^{III}-OOH Intermediate and Its Quantitative Conversion to an Fe^{IV}=O Complex. *J. Am. Chem. Soc.* **2011**, *133*, 7256–7259.

(20) (a) Magherusan, A. M.; Kal, S.; Nelis, D. N.; Doyle, L. M.; Farquhar, E. R.; Que, L., Jr.; McDonald, A. R. A $Mn^{II}Mn^{III}$-Peroxide Complex Capable of Aldehyde Deformylation. *Angew. Chem., Int. Ed.* **2019**, *58*, 5718–5722. (b) Yun, S.; Kwon, N.; Kim, S.; Jeong, D.; Ohta, T.; Cho, J. Reactivity Difference in the Oxidative Nucleophilic Reaction of Peroxonickel(III) Intermediates with Open-Chain and Macrocyclic Systems. *Inorg. Chem. Front.* **2019**, *6*, 2112–2117. (c) Zhang, Q.; Bell-Taylor, A.; Bronston, F. M.; Gorden, J. D.; Goldsmith, C. R. Aldehyde Deformylation and Catalytic C-H Activation Resulting from a Shared Cobalt(II) Precursor. *Inorg. Chem.* **2017**, *56*, 773–782. (d) Kim, J.; Shin, B.; Kim, H.; Lee, J.; Kang, J.; Yanagisawa, S.; Ogura, T.; Masuda, H.; Ozawa, T.; Cho, J. Steric Effect on the Nucleophilic Reactivity of Nickel(III) Peroxo Complexes. *Inorg. Chem.* **2015**, *54*, 6176–6183. (e) Geiger, R. A.; Chattopadhyay, S.; Day, V. W.; Jackson, T. A. Nucleophilic Reactivity of a Series of Peroxomanganese(III) Complexes Supported by Tetradentate Aminopyridyl Ligands. *Dalton Trans.* **2011**, *40*, 1707–1715.

(21) Luo, Y.-R. *Comprehensive Handbook of Chemical Bond Energies*, CRC Press: Boca Raton, FL, 2007.

(22) We propose a mechanism for the C-H bond activation by **1** as follows: A substrate H-atom abstraction by **1** occurs to form a putative iron(II)-hydroperoxo species, followed by the hydroperoxide O-O bond cleavage of the iron(II)-hydroperoxo species to form an iron(IV)-oxo complex. Although the proposed iron(IV)-oxo product was not detected in the reaction solution, one reviewer suggested that this iron(IV)-oxo complex might also be involved in the oxidation of organic substrates to give hydroxylated products. Further experiments, including ^{18}O-labeled water experiment by in situ prepared $[Fe(IV)(O)(13\text{-}TMC)]^{2+}$, are underway in this laboratory.

(23) It should be noted that metal-oxo complexes are known to exchange their O-atom with $H_2{}^{18}O$ prior to O-atom transfer to organic substrates. We performed OAT reaction of **1** with thioanisole in the presence of 10 μL of $H_2{}^{18}O$. Product analysis showed no incorporation of ^{18}O into the methyl phenyl sulfoxide product, suggesting that an iron(IV)-oxo species is not involved in the OAT reaction.

(24) The ET equilibrium constant (K_{et}) between **1** and ferrocene (Fc) was determined to be 27 from the ET titration of **1** with Fc as shown in Figure S20. The one-electron reduction potential (E_{red}) of **1** was determined to be 0.44 V vs SCE from the K_{et} value and the one-electron oxidation potential (E_{ox}) of Fc (E_{ox} = 0.37 vs SCE) using the Nernst equation. Surprisingly, E_{red} value of **1** is even higher than that of iron(IV)-oxo with 14-TMC, $[Fe^{IV}(O)(14\text{-}TMC)]^{2+}$ (E_{red} = 0.39 vs SCE[23a]), although E_{red} value of **1** is somewhat lower than that of corresponding iron(IV)-oxo, $[Fe^{IV}(O)(13\text{-}TMC)]^{2+}$ (E_{red} = 0.61 vs SCE[23b]). We suggest that the electrophilic reactivity of **1** may be resulted from the high reduction potential of **1**.

(25) (a) Lee, Y.-M.; Kotani, H.; Suenobu, T.; Nam, W.; Fukuzumi, S. Fundamental Electron-Transfer Properties of Non-heme Oxoiron(IV) Complexes. *J. Am. Chem. Soc.* **2008**, *130*, 434-435. (b) Hong, S.; So, H.; Yoon, H.; Cho, K.-B.; Lee, Y.-M.; Fukuzumi, S.; Nam, W. Reactivity Comparison of High-Valent Iron(IV)-Oxo Complexes Bearing N-Tetramethylated Cyclam Ligands with Different Ring Size. *Dalton Trans.* **2013**, *42*, 7842-7845.